Ordered Structure in Mixtures of a Block Copolymer and Homopolymers. 2. Effects of Molecular Weights of Homopolymers

Takeji Hashimoto,* Hideaki Tanaka,† and Hirokazu Hasegawa

Department of Polymer Chemistry, Kyoto University, Kyoto 606, Japan

Received October 24, 1989; Revised Manuscript Received March 26, 1990

ABSTRACT: Ordered microdomain structures for binary mixtures of a poly(styrene-*b*-isoprene) diblock copolymer (SI) with homopolystyrenes (HS) were investigated as a function of molecular weight of HS (M_{homo}) under conditions where the majority of HS can be solubilized into the polystyrene microdomains. For a given fraction of HS, the interdomain distance D was found to increase with M_{homo}, and a unique morphological transition from cylinders to lamellae was also found with increasing M_{homo}. These results imply that HS is generally not miscible with the polystyrene (PS) block chains confined in the microdomain space, although they are chemically identical. The higher the value M_{homo}, the lower the miscibility with the block PS chains. As a consequence, HS with higher M_{homo} tends to cause the PS microdomains to swell less uniformly, resulting in segregation more toward the middle of the PS microdomains. Here the conformational entropy loss upon mixing plays a dominant role in the miscibility of HS and block PS and hence on solubilization of HS into PS microdomains. Thus the miscibility of the confined chains is distinctly different from that of the corresponding free chain.

I. Introduction

In a previous paper[1] of this series of studies we reported the solubilization phenomenon of low molecular weight homopolymers (homopolystyrene (HS) and/or homopolyisoprene (HI)) into the microdomain of a poly(styrene-*b*-isoprene) diblock copolymer (SI). We found the following experimental evidence or implications. (i) The low molecular weight homopolymers HS and HI cause, more or less, the microdomain space to swell uniformly, resulting in expansion of the average distance between the neighboring chemical junctions of SI at the interface. (ii) The uniform swelling generally changes the microdomain morphology when an offset of the monomer composition of styrene and isoprene is induced by the addition of the homopolymers. (iii) A uniform solubilization was attained up to very high homopolymer content, at least as high as 80 wt %. (iv) The long-range spatial order of the microdomains was conserved down to a level at least as low as 20 wt % of block copolymer content in both the binary and ternary mixtures.

We have investigated the effect of the molecular weight of the homopolymer on the solubilization mechanism and hence on the morphology of ordered microdomains in the strong-segregation limit. We report the results on a binary mixture of HS and SI. Here again we restrict the molecular weight of HS to such a low molecular weight range that all of the HS molecules are essentially solubilized into the polystyrene (PS) microdomains formed by SI, as will be clarified in section IV.3.

The Discussion (section IV) consists of five sections. In section IV.1 we analyze the thermodynamic stability of our SI/HS binary mixtures for the macrophase and microphase transitions to clarify the microphase transitions dominating the structure formation of our systems. In section IV.2 we perform a paracrystal analysis of the SAXS profiles to determine the change in lamellar thickness of both polystyrene and polyisoprene lamellae upon addition of HS. In section IV.3 we analyze homopolymer fractions solubilized into the microdomain space, and in section IV.4 we analyze the solubilization behavior of homopolymers, e.g., "localized solubilization" vs "uniform solubilization", as a function of their molecular weights. In section IV.5 we compare our results with some interesting results previously reported by Koberstein et al.[2,3]

II. Experimental Methods

An SI block polymer (HY-8) and a series of HS (S17, S10, S04, and S02) were prepared by a living anionic polymerization technique described in detail elsewhere.[1] They are listed in Table I, where S stands for HS and the two digits after S denote their M_n (number-average molecular weight) in units of thousands. SI/HS mixtures were dissolved in toluene (a common solvent), the total polymer concentration being 10 wt %, and cast into film specimens by slowly evaporating the solvent over 4 weeks at 30 °C. After 4 weeks, the specimens were further dried in a vacuum oven to remove residual solvent until a constant weight was attained. For each HS, film specimens were prepared from 80/20 and 50/50 wt %/wt % mixtures of SI/HS. No further annealing was performed on the test specimens. There are some nonequilibrium effects of the kind described previously[4] on the morphology of as-cast films. However, these nonequilibrium effects will affect neither the qualitative discussion on the solubilization given later in section IV.1 nor the discussion in section IV.4 and hence the conclusions in section V.

The microdomain structures existing in the film specimens were investigated by small-angle X-ray scattering (SAXS) at room temperature. The SAXS measurements were conducted in the same manner as described elsewhere.[1]

III. Results

Figures 1 and 2 show SAXS profiles for pure SI block polymer (HY-8) and mixtures of HY-8 and HS, i.e., HY-8/S02, HY-8/S04, HY-8/S10, and HY-8/S17. HY-8 and HS are mixed with a composition of 80/20 wt %/wt % (Figure 1) and 50/50 wt %/wt % (Figure 2). In these figures, 2θ is the scattering angle, and s is the magnitude of the scattering vector defined by

$$s = (2 \sin \theta)/\lambda$$

where λ is the wavelength of the X-rays in the medium, the monochromatized Cu Kα line of $\lambda = 0.154$ nm being used in this experiment.

Let us first examine the results obtained in Figure 1. All of the HY-8/HS mixtures with 80/20 wt %/wt %

† Present address: Mitsubishi Kasei Corp., Research Center, 1000 Kamoshida-cho, Midori-ku, Yokohama 227, Japan.

0024-9297/90/2223-4378$02.50/0

Table I
Molecular Characteristics of Block Copolymer HY-8 and Homopolymers HS (S17, S10, S04, and S02)

specimen	$M_n \times 10^{-3}$ [a]	S/I (wt %/wt %)[b]	M_w/M_n[c]
HY-8	31.6	48/52	1.07
S17	16.7	100/0	1.02
S10	10.2	100/0	1.02
S04	4.4	100/0	1.06
S02	2.3	100/0	1.10

[a] Determined by membrane osmometry or vapor pressure osmometry. [b] Determined by elemental analysis. [c] Determined by size exclusion chromatography.

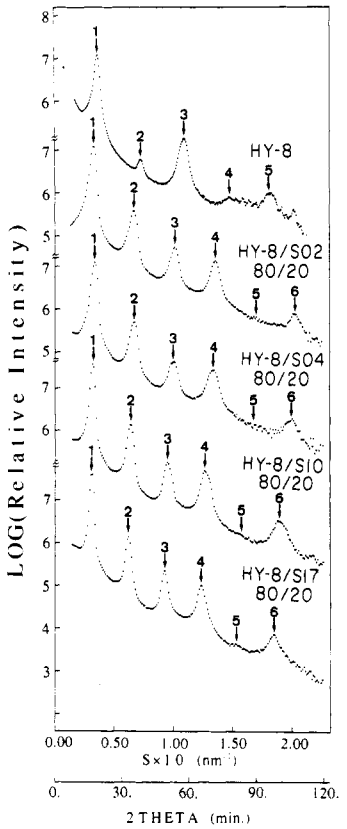

Figure 1. SAXS profiles from HY-8 and the 80/20 (wt %/wt %) mixtures of HY-8/HS. For HS, the two digits after S denote the M_n of homopolystyrene in units of thousands. All of the profiles show five or six scattering peaks at scattering angles of integer multiples of that of the first-order peak, indicating the lamellar microdomain morphology.

composition as well as HY-8, pure diblock polymer SI, exhibit scattering profiles relevant to the alternating polystyrene (PS) and polyisoprene (PI) lamellar microdomains, showing higher order scattering maxima at positions of integer multiples of s of the first-order scattering maximum. All of the mixtures as well as HY-8 have a long-range spatial order of lamellae as indicated by the existence of the scattering maxima at least up to the sixth order.

The relative peak heights of the higher order maxima of the mixtures are nearly identical but are drastically different from those of the pure block polymer HY-8. Since the relative peak heights of the higher order SAXS maxima are known to be a function of volume fraction of one type of lamellar microdomain,[5,6] the change of the relative peak heights with the addition of HS indicates the change in relative volume of the two types of lamellae (i.e., PS and PI lamellae) with HS, which, in turn, implies definitely and nicely a solubilization of HS into the lamellar microdomain space. The fact that the relative peak heights are

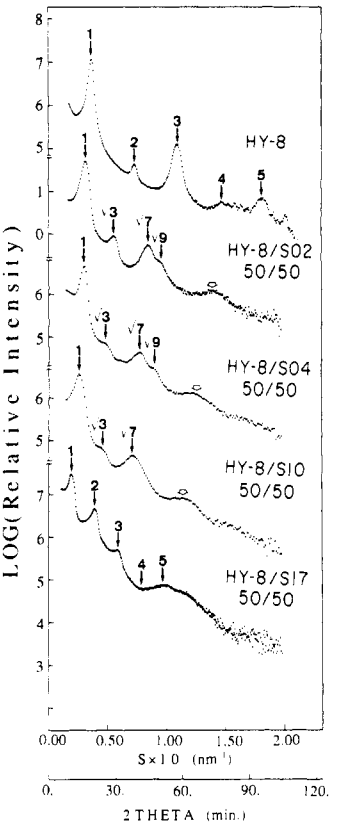

Figure 2. SAXS profiles from HY-8 and the 50/50 wt %/wt % mixtures of HY-8/HS. HY-8 and HY-8/S17 show scattering profiles characteristic of the lamellar microdomain morphology, while the other mixtures show scattering profiles characteristic of the hexagonally packed cylindrical microdomain morphology with the scattering peak positions in the ratio of $1:\sqrt{3}:\sqrt{4}:\sqrt{7}:\sqrt{9}$, the peak of $\sqrt{4}$ being suppressed due to a special volume fraction of the polyisoprene cylinders.

identical for all of the mixtures implies that the total amount of HS solubilized in the microdomain space is invariant with molecular weight of HS. From the experimental results shown in Figure 1, one can extract information on the change of polystyrene (PS) and polyisoprene (PI) lamellae with HS as a function of molecular weight of HS. Thus one can analyze how HS solubilizes into the microdomain space of SI.

Figure 2 shows the SAXS profiles for mixtures containing a higher fraction of HS. The 50/50 mixtures of HY-8/S02, HY-8/S04, and HY-8/S10 exhibit scattering profiles relevant to the morphology of hexagonally packed cylindrical microdomains, having the first and higher order maxima at the scattering vectors s of 1, $\sqrt{3}$, $\sqrt{7}$, $\sqrt{9}$, ... relative to that for the first-order maximum. The broad scattering maximum shown by the thick arrow is due to the second-order maximum from the isolated cylinders ($n = 2$ in eq III-4). Thus a larger amount of HS solubilized into the microdomains changes the morphology from alternating lamellae to the hexagonally packed cylinders. It should be noted that the long-range order is still conserved upon addition of an equal amount of homopolymer.

A spectacular feature appears upon increasing the molecular weight of HS as seen for the HY-8/S17 mixture. The mixture shows a profile relevant to the lamellar microdomain, having higher order maxima at the scattering vectors s of integer multiples of that of the first-order maximum. Thus upon increasing the molecular weight of HS, the original lamellar microdomain is surprisingly recovered. It is important to note here that HS (S17) is still solubilized into the microdomain space, as shown in

Table II
Characterization of Microdomain Structures for 80/20 wt %/wt % HY-8/HS Mixtures

sample	morphology	interdomain dist D, nm	D/D_0[a]	ρ_J/ρ_{J0}[b]	a_J/a_{40}[c]	D_{PS},[d] nm	D_{PI},[d] nm
HY-8	lamellar	26.7	1	1	1	12.6	14.1
HY-8/S02	lamellar	29.3	1.10	0.876	1.068	17.3	12.0
HY-8/S04	lamellar	30.5	1.14	0.913	1.047	18.0	12.5
HY-8/S10	lamellar	31.3	1.17	0.938	1.033	18.5	12.8
HY-8/S17	lamellar	31.9	1.19	0.953	1.024	18.8	13.1

[a] The interdomain distance relative to that for pure block polymer HY-8 (D_0 = 26.7 nm). [b] The average density of chemical junction points along the interfaces of the microdomains relative to that for pure block polymer HY-8 (ρ_{J0} = 0.251 nm^{-2}) as estimated from eq IV-9. [c] The average nearest-neighbor distance between chemical junction points along the interfaces relative to that for pure block polymer HY-8 (a_{J0} = 2.00 nm). $a_J/a_{J0} = (\rho_{J0}/\rho_J)^{1/2}$. [d] The average lamellar thickness for PS microdimains (D_{PS}) and PI microdomains (D_{PI}) as determined from the paracrystal analysis described in the text (section IV.2).

Table III
Characterization of Microdomain Structures for 50/50 wt %/wt % HY-8/HS Mixtures

sample	morphology	interdomain dist D, nm	D/D_0	ρ_J/ρ_{J0}	a_J/a_{J0}	D_{PS}, nm	D_{PI}, nm	R,[a] nm
HY-8	lamellar	26.7	1	1	1	12.6	14.1	
HY-8/S02	cylindrical	35.6	1.312	0.657	1.233			9.5
HY-8/S04	cylindrical	37.9	1.416	0.709	1.187			10.7
HY-8/S10	cylindrical	43.6	1.629	0.816	1.107			11.9
HY-8/S17	lamellar	51.0	1.935	0.968	1.017	37.5	13.5	

[a] Average radius of cylindrical microdomains as determined by SAXS (eq III-4). D/D_0, ρ_J/ρ_{J0}, a_J/a_{J0}, D_{PS}, and D_{PI} have the same meanings as in Table II.

the shift of the scattering peak positions toward smaller angles, compared with those for pure block polymer HY-8, and the change of relative peak heights with the addition of S17.

Tables II and III summarize the results obtained in Figures 1 and 2 on morphology, average interdomain distance D, and average radius of the cylindrical domain R. Here D values for the lamellar microdomains were determined by

$$2D \sin \theta_{\max,n} = n\lambda \quad \text{(for lamellae)} \qquad \text{(III-1)}$$

where $2\theta_{\max,n}$ is the scattering angle where the nth-order maximum locates. D can be determined with a high precision by taking an average of D's estimated from a number of the higher order maxima. For the hexagonally packed cylindrical domains D was determined from

$$2d_{hk0} \sin \theta_{m,hk0} = \lambda \qquad \text{(III-2)}$$

$$d_{hk0} = D/[(4/3)(h^2 + hk + k^2)]^{1/2} \qquad \text{(III-3)}$$

where $2\theta_{m,hk0}$ is the scattering maximum at which the diffraction maximum from the ($hk0$) plane occurs, and d_{hk0} is the lattice spacing of the ($hk0$) plane. The average radius R was obtained from the scattering maximum originating from the isolated cylinders

$$(4\pi/\lambda)R \sin \theta_{\max,n} = 4.98, 8.364, 11.46, \ldots \qquad \text{(III-4)}$$

for n = 1, 2, 3, etc., respectively. The maximum marked by an arrow in Figure 2 corresponds to that for n = 2. The value R thus estimated turned out to be reasonable from volumetric considerations. The volume fraction of the PI cylinders, $\phi_{PI,SAXS}$ is given by

$$\phi_{PI,SAXS} = (2\pi/3^{1/2})(R/D)^2 \qquad \text{(III-5)}$$

$\phi_{PI,SAXS}$ can thus be estimated from R and D, which, in turn, are determined from the SAXS profile. This value of $\phi_{PI,SAXS}$ is in good agreement with $\phi_{PI,vol}$ as estimated from the composition of the binary mixture of SI/HS

$$\phi_{PI,vol} = f(1 - \phi_H) \qquad \text{(III-6)}$$

where f is the volume fraction of PI block chain in SI diblock polymer and ϕ_H is the volume fraction of HS in the microdomain space. The value of R turned out to be reasonable also from the theoretical analyses of the scattering profile based on a paracrystal model.[7] D/D_0 in Tables II and III indicates the change of the interdomain distance D with the addition of HS normalized by the interdomain distance of pure SI (D_0). The rest of the parameters in the tables were obtained as a result of the analyses discussed in section IV.2.

IV. Discussion

1. Microphase Transition and Macrophase Transition. Since the SI/HS mixtures have generally two kinds of phase transitions[8-13] ((i) the liquid–liquid phase separation between SI and HS, which we call the "macrophase transition", and (ii) the order–disorder transition, which we call the "microphase transition"), it may be useful to estimate spinodal lines for the two kinds of transitions in order to foresee the possibility of solubilization. Solubilization is expected to occur if the microphase transition occurs prior to the macrophase transition by lowering the temperature of the mixtures or by increasing the polymer concentration of the mixtures with a solvent from a single-phase state.

The thermodynamic stability limits of the mixtures (i.e., spinodal points) were estimated in the context of the mean-field random phase approximation as described elsewhere.[11-13] Figure 3 shows the value χN at spinodal points $(\chi N)_s$ as a function of the volume fraction of the block polymer SI (ϕ_{block}), where χ is the Flory interaction parameter between PS and PI per monomer unit and N is the degree of polymerization of SI. In each diagram the solid and broken lines indicate, respectively, the $(\chi N)_s$ for the macrophase and microphase transitions.

In the regions between the microphase and macrophase transitions, the mixtures are unstable for the microphase transition but stable or metastable for the macrophase transition. Hence the mixtures tend to form microdomains, and HS tends to be solubilized into the PS domains. Lowering the temperature from the single-phase state or increasing the polymer concentration (with a neutral solvent) from the single-phase state corresponds to increasing χN from the point below the spinodal line

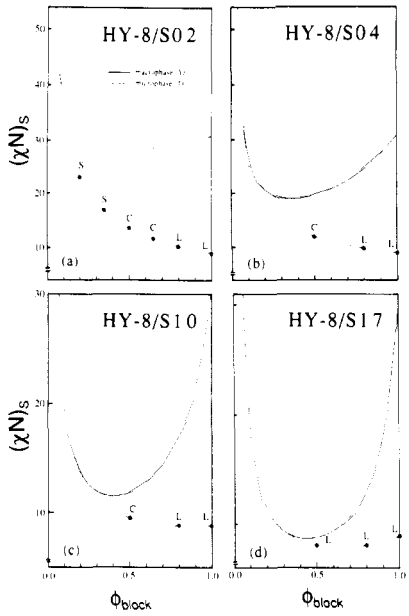

Figure 3. Calculated spinodal points $(\chi N)_s$ for macrophase transition (solid lines) and microphase transition (broken line) as a function of the volume fraction of the SI block polymer ϕ_{block}. (a) HY-8/S02; (b) HY-8/S04; (c) HY-8/S10; (d) HY-8/S17. N/N_H = 20.4, 10.6, 4.59, and 2.80 for the mixtures shown in parts a–d, where N and N_H are the degrees of polymerization of HY-8 and HS, respectively.

$(\chi N)_s$ for the microphase transition. All of the SI/HS mixtures with $\phi_{block} > 0.5$ have $(\chi N)_s$ for the microphase transition lower than that for the macrophase transition, and hence HS may be solubilized into the microdomains. The symbols S, C, and L in Figure 3 stand for spherical, cylindrical, and lamellar microdomain morphologies, respectively, which were observed for the as-cast films having corresponding ϕ_{block} at room temperature.

2. Analyses of SAXS Profiles Based upon the Paracrystal Model. In this section we analyze the SAXS profiles from the lamellar microdomains based on a model of one-dimensional paracrystal with uniaxial orientation to determine the volume fraction of one of the microdomains, e.g., PI lamellae ϕ_{PI} and its change with addition of HS. If one can determine both ϕ_{PI} and D, one can estimate D_{PI} and D_{PS}, the thicknesses of the PI and PS lamellae, respectively, since

$$\phi_{PI} = D_{PI}/(D_{PS} + D_{PI}) = D_{PI}/D \qquad \text{(IV-1)}$$

The evaluations of D_{PI} and D_{PS} are quite useful to explore solubilization behavior and mechanism. The principles and methods of paracrystal analyses have been described in detail elsewhere[6] and need not be repeated here. Similar paracrystal analyses can be done for the cylindrical domains hexagonally packed in space.[7] However, the paracrystal analyses of the cylindrical domains will not be discussed here, since the estimations of R and D are sufficient to explore the solubilization behavior and mechanism for such cylinders, and R and D can be estimated without employing paracrystal analyses.

We performed paracrystal analyses on all of the specimens showing lamellar microdomains (see Tables II, III, and V). Here we show the results for HY-8/S17 (50/50 wt %/wt %) as a typical example in Figures 4–6. Each scattering profile shown by the data points in Figures 4–6 is an experimental profile obtained by irradiation with the incident X-ray beam parallel to the film surfaces and by scanning the scattered X-ray beam normal to the film surfaces. The profile shown by the solid line in Figure 4 is the theoretical profile best fitted with the experimental

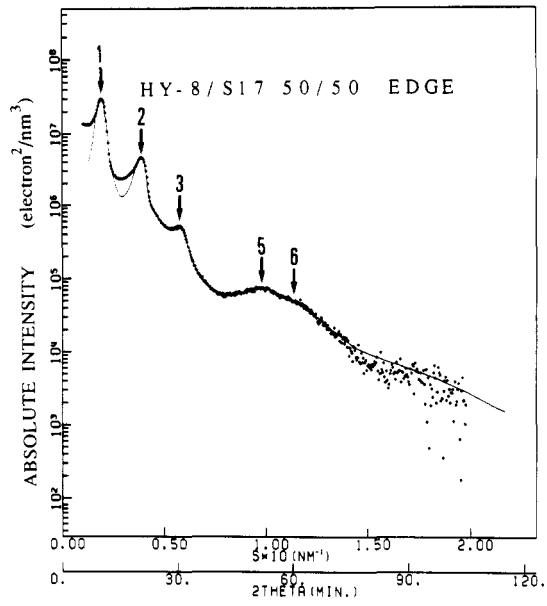

Figure 4. Best-fit theoretical (solid line) and experimental SAXS profile (profile shown by data points) for HY-8/S17 50/50 wt %/wt % mixture. The best fit was obtained for D = 51.0 nm, g = 0.08, ϕ_{PI} = 0.265, σ_{PI} = 1.0 nm, and t = 2.5 nm.

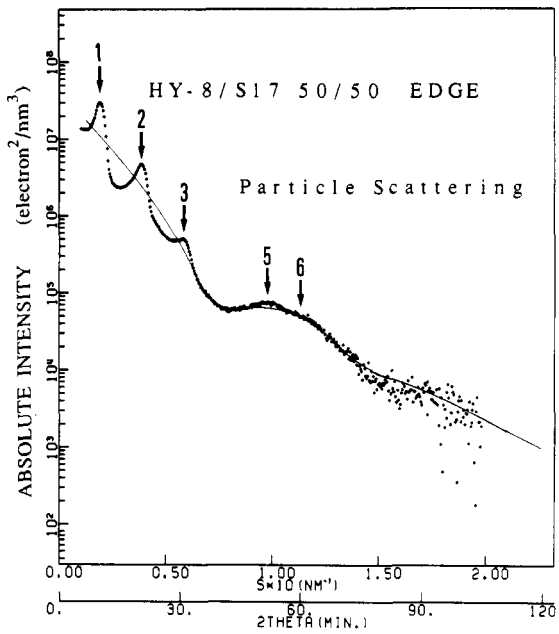

Figure 5. Best-fit theoretical particle scattering function (solid line) and experimental SAXS profile (profile shown by data points) for HY-8/S17 50/50 wt %/wt % mixture. The best fit was obtained for ϕ_{PI} = 0.265, σ_{PI} = 1.0 nm, and t = 2.5 nm.

profile. The best fit gives the following fundamental parameters characterizing the paracrystal model: D = 51.0 nm, g = 0.08, ϕ_{PI} = 0.265, σ_{PI} = 1.0 nm, and t = 2.5 nm, where D is the average interdomain distance, g is the paracrystal distortion factor defined by

$$g \equiv \Delta D/D \qquad \text{(IV-2)}$$

ΔD being the standard deviation of the interdomain distance, ϕ_{PI} is the volume fraction of the PI lamellae, σ_{PI} is the standard deviation of the thickness of the PI lamellae, and t is the interfacial thickness characterizing the composition profile across the lamellar interface.[5,6,14,15] It should be noted that the volume fraction obtained by the paracrystal analyses refers to that for either the PS or PI domain, because of the reciprocity principle of scattering. It was identified to be that of the PI lamellae by volumetric considerations.

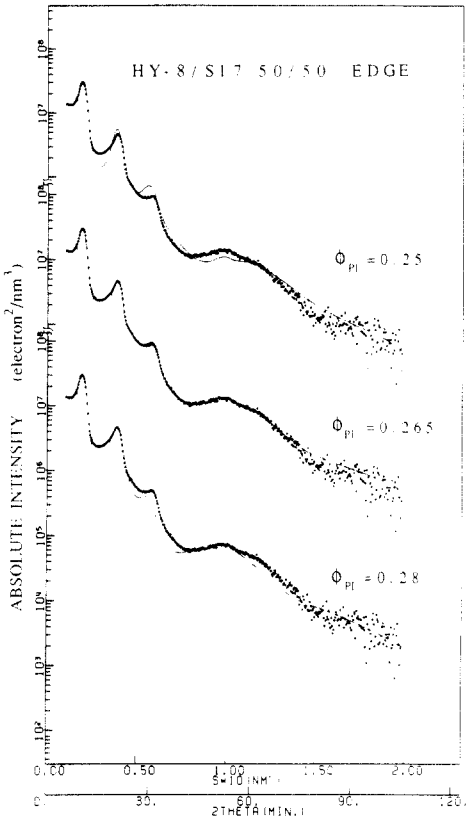

Figure 6. Comparison of theoretical scattering functions and experimental SAXS profiles (profiles shown by data points) for HY-8/S17 50/50 wt %/wt % mixture. The theoretical profiles for ϕ_{PI} = 0.250, 0.265, and 0.280 are compared with the given experimental profile. Other parameters were fixed at D = 51.0 nm, g = 0.08, σ_{PI} = 1.0 nm, and t = 2.5 nm.

A number of the fundamental parameters could be more or less uniquely determined owing to the existence of a number of higher order peaks up to the sixth order, with the fourth-order peak being much suppressed, and owing to the fact that each parameter affects the profile differently: D affects the peak position, g affects the number of higher order diffraction maxima, ϕ_{PI} affects relative peak heights as will be demonstrated in Figure 6, σ_{PI} damps the higher order maxima, in a manner similar to the g factor but σ_{PI} is more sensitive to the higher order peaks than g, and t affects the q dependence of the scattering profile at larger scattering angles. As t increases, the scattering profile at the large-angle tail tends to decay more rapidly with q. Tables II and III show the values of D_{PS} and D_{PI} determined from the estimated values of ϕ_{PI} and D as a result of such paracrystal analyses.

The profile shown by the solid line in Figure 5 was obtained by calculating the particle scattering $\langle f_L^2 \rangle$ for one of the lamellar domains with $D_{PI} = \phi_{PI}D = 0.265 \times 51.0$ nm = 13.5 nm, σ_{PI} = 1.0 nm, and t = 2.5 nm. Here f_L^2 is the structure factor for a single lamella given by

$$f_L^2 = Z^2[\sin^2(\pi sz)/(\pi sz)^2] \exp(-4\pi^2\sigma^2 s^2) \quad \text{(IV-3)}$$

where z is the thickness of the lamella and σ is the parameter related to t by

$$t = (2\pi)^{1/2}\sigma \quad \text{(IV-4)}$$

$\langle f_L^2 \rangle$ is the average structure factor of the isolated lamella given by

$$\langle f_L^2 \rangle = \int_{z=0}^{\infty} f^2 P(z)\, dz \Big/ \int_{z=0}^{\infty} P(z)\, dz \quad \text{(IV-5)}$$

where $P(z)$ is the distribution function for the particle thickness z

$$P(z) \sim \exp[-(z - D_{PI}^2)/2\sigma_{PI}^2] \quad \text{(IV-6)}$$

Comparison of the calculated particle scattering profile and the experimental profile reveals that the broad peak centered around s = 0.1 nm^{-1} is due to the first-order scattering peak from the isolated PI lamella, on top of which are superimposed the fifth- and sixth-order Bragg diffractions from the lamellar identity period D. It is very rare and unique that the higher order maxima from the isolated lamella are observed for the regular assemblies of such lamellae. This is the consequence of a combination of a small g and a small σ_{PI}.

Figure 6 highlights the effect of ϕ_{PI} on the calculated scattering profiles for a fixed set of parameters: D = 51.0 nm, g = 0.08, σ_{PI} = 1.0 nm, and t = 2.5 nm. The relative peak heights are clearly seen to change very sensitively with ϕ_{PI}. The best fit is obtained for ϕ_{PI} = 0.265.

3. Solubilization of Homopolymers in the Microdomain Space. We analyze here the amount of HS solubilized into the microdomain space. We assume here that HS is selectively solubilized into PS domains but not in PI domains.

From volumetric considerations, the radius of the PI cylinder R ($R_{PI,vol}$) can be estimated from the intercylinder distance D, average volume fraction of HS solubilized in the microdomain space ϕ_H, and volume fraction of PI chain in SI block polymer f

$$R_{PI,vol} = [3^{1/2}(1 - \phi_H)f/2\pi]^{1/2}D \quad \text{(IV-7)}$$

This radius can be compared with the radius $R_{PI,SAXS}$ directly determined by the SAXS profile using eq III-4 to estimate ϕ_H from D determined by SAXS (eq III-3) and f determined by the chemistry of the block polymer. Similarly the thickness of the PS lamella $D_{PS,vol}$ can be calculated from volumetric considerations

$$D_{PS,vol} = D[1 - f(1 - \phi_H)] \quad \text{(IV-8)}$$

This value of $D_{PS,vol}$ can be compared with $D_{PS,SAXS}$ as determined by the paracrystal analyses in section IV.2.

Let us first assume that all of the homopolymers HS are solubilized into the PS domain so that ϕ_H is equal to the volume fraction as calculated from the composition of a given mixture of SI/HS. Under this assumption $R_{PI,vol}$ and $D_{PS,vol}$ were calculated by using eqs IV-7 and IV-8 and summarized, respectively, in Tables IV and V. $R_{PI,vol}$ and $D_{PS,vol}$ are in good agreement with $R_{PI,SAXS}$ and $D_{PS,SAXS}$, respectively. This indicates that all of the homopolymers tend to be solubilized somewhere in the microdomain space under the solution-cast method employed in this work. In the next section we further examine the solubilization behavior of HS into the PS microdomains, i.e., localized vs uniform solubilization.

4. Swelling of Microdomains by Homopolymers. In the case of the uniform solubilization of HS, HS tends to

Table IV
Comparisons between the Measured and Calculated Radii of the PI Cylinders

sample	comp, wt %/wt %	radius, nm	
		$R_{PI,SAXS}$[a]	$R_{PI,vol}$[b]
HY-8/S02	50/50	9.5	9.8
HY-8/S04	50/50	10.7	10.3
HY-8/S10	50/50	11.9	11.8

[a] Radius of PI cylinder as determined by SAXS (eq III-4). [b] Radius of PI cylinder as determined by volumetric considerations with the assumption of a complete solubilization of HS into the PS matrix (eq IV-7).

Table V
Comparisons of Thickness of PS Lamella As Determined by SAXS with That As Calculated by Volume

sample	comp, wt %/wt %	D_{PS}, nm	
		$D_{PS,SAXS}$[a]	$D_{PS,vol}$[b]
HY-8/S02	80/20	17.3	16.9
HY-8/S04	80/20	18.0	17.6
HY-8/S10	80/20	18.5	18.1
HY-8/S17	80/20	18.8	18.4
HY-8/S17	50/50	37.5	37.5

[a] PS lamellar thickness as determined by the paracrystal analysis (section IV.2). [b] PS lamellar thickness as determined by volumetric considerations with the assumption of a complete solubilization of HS into the PS lamellar microdomains (eq IV-8).

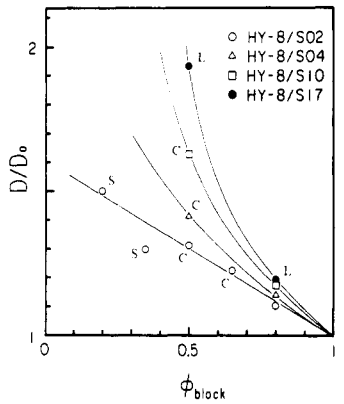

Figure 7. Average interdomain distance relative to that for pure block polymer HY-8 (D_0 = 26.7 nm) D/D_0 as a function of volume fraction of block polymer ϕ_{block} for mixtures with various HS having different molecular weights. L, C, and S beside the data points designate lamellar, cylindrical, and spherical microdomain morphologies, respectively.

cause the PS domains to swell in the directions both parallel and perpendicular to the interface, causing changes in molecular conformations of both homopolymers and block polymer chains and a change in the density of the chemical junctions of the block chains ρ_J along the interface (Figure 12a,b). On the other hand, in the case of the localized solubilization of HS in the middle of the PS microdomains, the conformations of PI block chains and the interfacial density of the chemical junctions of the block chains do not necessarily change with the solubilization (Figure 12a,d).[17] In this section, we analyze such solubilization behavior of HS in the PS domains. Uniform solubilization implies a high degree of miscibility between HS and PS chains, giving rise to a more or less uniform spatial segmental density profile of HS (Figure 12b). On the other hand, localized solubilization implies a low degree of miscibility between HS and PS chains, giving rise to a nonuniform spatial segmental density profile of HS (Figure 12d).

Figure 7 shows the ratio of the interdomain distances D/D_0 as a function of volume fraction ϕ_{block} of the block polymer SI in the mixtures with HS having different molecular weights where D_0 is the interdomain distance of pure block polymer HY-8 (D_0 = 26.7 nm). The symbols S, C, and L in the figure designate, respectively, the spherical, cylindrical, and lamellar morphologies. D increases with increasing $\phi_H = 1 - \phi_{block}$ for HS with a given molecular weight, clearly indicating the solubilization effect. For a given ϕ_H, D increases with increasing molecular weight of HS, implying that the solubilization behavior depends on molecular weight of HS for a given block polymer.

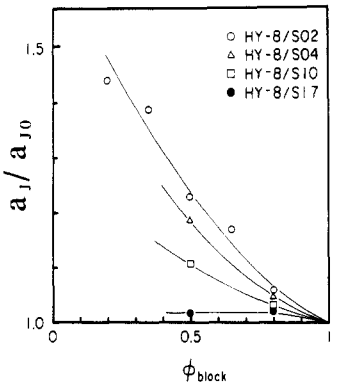

Figure 8. Average nearest-neighbor distance of chemical junction points along the interfaces of the microdomains relative to that for pure block polymer HY-8 (a_{J0} = 2.00 nm) a_J/a_{J0} plotted against the volume fraction of the block polymer ϕ_{block} for HY-8/HS blends.

Simple volumetric considerations give

$$D/D_0 = (\rho_J/\rho_{J0})\phi_{block}^{-1} \quad \text{(IV-9)}$$

for lamellar microdomains,

$$D/D_0 = (\rho_J/\rho_{J0})[(2/3^{1/2})\pi f\phi_{block}^{-1}]^{1/2} \quad \text{(IV-10)}$$

for hexagonally packed cylindrical microdomains, and

$$D/D_0 = (\rho_J/\rho_{J0})[(27(3^{1/2})/8)\pi f^2\phi_{block}^{-1}]^{1/3} \quad \text{(IV-11)}$$

for spherical microdomains in a body-centered cubic lattice, where ρ_{J0} is ρ_J for pure block polymer and ρ_J is the number of block chains per unit interfacial area. Since f and ϕ_{block} are known, $(\rho_J/\rho_{J0}) \cong (a_{J0}/a_J)^2$ can be estimated from D/D_0, where a_{J0} and a_J are the average nearest-neighbor distance between the chemical junctions along the interface before and after addition of the homopolymer.

Figure 8 shows the change of a_J/a_{J0} with $\phi_{block} = 1 - \phi_H$ for HS having various molecular weights. For a given molecular weight of HS, a_J/a_{J0} tends to expand with increasing ϕ_H and hence decreasing ϕ_{block}. This implies that HS tends to cause the PS domains to swell laterally, i.e., in a direction parallel to the interface. For a given ϕ_H, a_J/a_{J0} decreases and hence the degree of the lateral swelling decreases with increasing molecular weight of HS. The lower the degree of lateral swelling, the higher the value ρ_J/ρ_{J0} and hence the larger the expansion of the interdomain distance D/D_0 (eqs IV-9 to IV-11). The tendency can be clearly seen in Figure 9 for ϕ_{block} = 0.5 and in Figure 10 for ϕ_{block} = 0.8. It should be noted that R_{PI} increases with increasing ρ_J/ρ_{J0}

$$R_{PI}/R_{PI,0} = \rho_J/\rho_{J0} \quad \text{(IV-12)}$$

where $R_{PI,0}$ and ρ_{J0} are R_{PI} and ρ_J for the SI/HS mixture with the lowest molecular weight HS.

Figure 9 shows the change of the cylindrical microdomain with increasing molecular weight of HS, $M_{n,homo}$, for ϕ_{block} = 0.5. D and R_{PI} are the intercylinder distance and the radius of the PI cylinder as determined by SAXS. As $M_{n,homo}$ increases, a_J/a_{J0} decreases and hence ρ_J/ρ_{J0} increases, giving rise to an increase of D (eq IV-10). The increase of D also causes an increase of R_{PI} (eq IV-12) so that R_{PI}/D is kept constant (0.27–0.28) (see eq IV-7). Figure 10 shows the change of the lamellar microdomain with $M_{n,homo}$ for ϕ_{block} = 0.8 where $D_{PI,0}$ and $D_{PS,0}$ are the lamellar thicknesses for the PI and PS lamellae for pure SI block polymer. The dash–dot line in Figure 10 shows the value of $D_{PI,0}$, and D_{PS} and D_{PI} are the values determined by the paracrystal analyses of the SAXS profiles. It should be noted that the solubilization of HS into PS domains causes

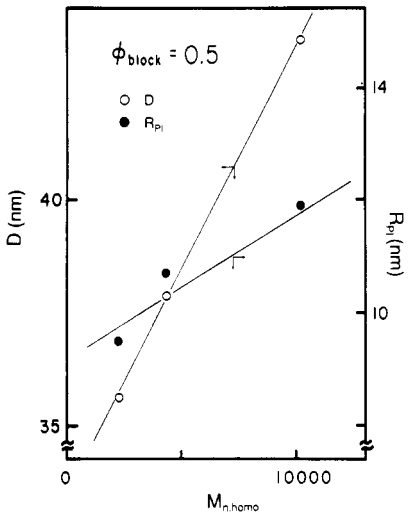

Figure 9. Average interdomain distance D and average radius of PI cylinders R_{PI} plotted against the number-average molecular weight of HS ($M_{n,homo}$) for the 50/50 wt %/wt % mixtures of HY-8/HS having cylindrical microdomain morphologies. D and R_{PI} are determined from the SAXS profiles (eqs III-3 and III-4).

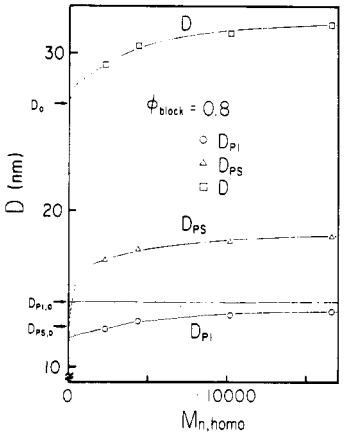

Figure 10. Average interdomain distance D, thickness of PS lamella D_{PS}, and thickness of PI lamella D_{PI} plotted against the number-average molecular weight of HS ($M_{n,homo}$) for the 80/20 wt %/wt % mixtures of HY-8/HS having lamellar microdomain morphologies. D was determined from SAXS profiles using eq III-1, and D_{PS} and D_{PI} were determined from the paracrystal analyses of the SAXS profiles.

a decrease of D_{PI}. This is interpreted as follows. The solubilization causes a decrease of ρ_J/ρ_{J0} as a consequence of the swelling so that it affects chain conformations and packing in PI lamellae. In order to maintain bulk density, PI chains tend to be less stretched normal to the interface, which, in turn, causes a decrease of D_{PI} with solubilization. It is worth noting that our preliminary studies on small-angle neutron scattering[16] imply that the uniform solubilization of HS causes further stretching of PS block chains perpendicular to the interface and that the uniformly solubilized HS also has a conformation stretched and squeezed in the directions perpendicular and parallel to the interface, respectively.

As $M_{n,homo}$ increases, the solubilization becomes less uniform, and hence the decrease of ρ_J/ρ_{J0} becomes small. This effect, in turn, causes D_{PI} to increase with increasing $M_{n,homo}$ toward the value $D_{PI,0}$. Figure 11 summarizes the molecular weight dependence of HS on the solubilization as appearing on the molecular weight dependence of D/D_0 (a) and a_J/a_{J0} (b) where the symbols C and L stand for the cylindrical and lamellar microdomains, respectively.

5. Further Comments. Koberstein and co-workers[2,3] reported some interesting preliminary results on the

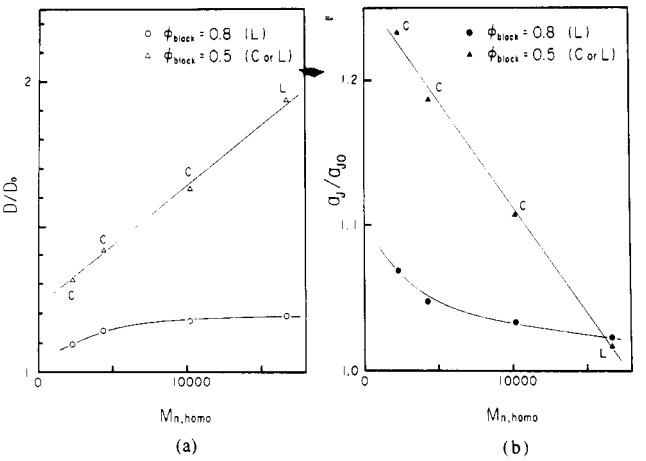

Figure 11. Average interdomain distance relative to that for pure block polymer HY-8 (D_0 = 26.7 nm) (D/D_0) (a) and average distance between the nearest-neighbor chemical junction points along the interfaces of the microdomains relative to that for pure block polymer HY-8 (a_{J0} = 2.00 nm) (a_J/a_{J0}) (b) plotted against the number-average molecular weight of HS ($M_{n,homo}$) for the 50/50 (triangles) and 80/20 (circles) wt %/wt % mixtures of HY-8/HS.

solubilization[2] of hydrogenated polybutadiene (hPB) into the matrix of poly(styrene-*b*-hydrogenated butadiene-*b*-styrene) (S-hB-S) triblock polymers as a function of molecular weight of hPB and on the spatial distribution of the solubilized hPB in the microdomain space of the hPB block chains.[3] They found a trend of increasing D/D_0 with increasing molecular weight of hPB in the lower molecular weight regime of hPB.[2] This trend is consistent with our results, as clearly shown in Figures 9–11. However, we could not confirm at all the puzzling result on $D/D_0 < 1$ that they reported for the lowest molecular weight hPB. Our results show that the swelling of one of the microdomains (e.g., PS) by homopolymers (e.g., HS) always gives $D > D_0$, though $D_{PI} < D_{PI,0}$ and $D_{PS} > D_{PS,0}$. They also reported a trend of the solubilized hPB hompolymers being localized in the center of the microdomain space of the hPB block chains by simultaneous SAXS and small-angle neutron scattering measurements on the same specimens. This trend is consistent with our finding on the localized solubilization of HS into the PS microdomain system. The amount of homopolymers solubilized in the corresponding microdomain space and ϕ_{homo}, the spatial distribution of the homopolymers in the solubilized domains, depend on the molecular architecture, e.g., triblock vs diblock polymers, and the segregation power χN_B and/or χN_H, where χ is the Flory interaction parameter per monomer unit between dissimilar polymers, and N_B and N_H are the polymerization indices for the block polymer and homopolymer, respectively.

V. Conclusions

All of the homopolystyrenes (HS) studied were found to be solubilized into the PS microdomains under the solution-cast method employed in this work. The molecular weight of HS, $M_{n,homo}$, covered in this work is about equal to or less than that of the polystyrene block chains. Figure 12 schematically summarizes the solubilization behavior of HS into the PS microdomains, where part a shows the lamellar microdomain of pure SI block polymer and parts b–d show the effects of solubilization of HS on the microdomains and the spatial segmental density profile of HS, ϕ_{homo}. The effect of molecular weight of HS, $M_{n,homo}$, on ϕ_{homo} is somewhat exaggerated in order to schematically highlight its effect.

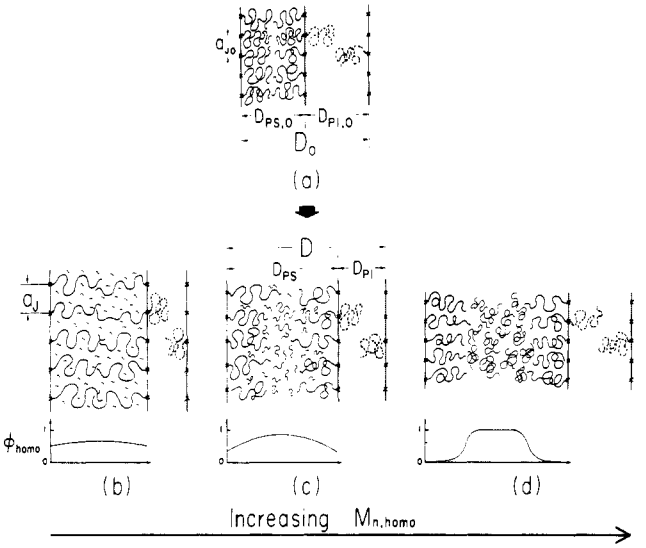

Figure 12. Schematic representations of the spatial segmental distributions of the block polymer and homopolystyrene chains in a microdomain space for different states of solubilization and corresponding spatial segmental density profile of HS (ϕ_{homo}) across the PS microdomain space: (a) pure block polymer; (b) uniform solubilization of HS in the PS microdomain; (c) intermediate state between b and d; (d) localized solubilization of HS in the center of the PS microdomain. The molecular weight of HS ($M_{n,homo}$) increases in the order of b, c, and d. The solubilization generally involves changes of a_{J0}, $D_{PS,0}$, $D_{PI,0}$, and D_0 into a_J, D_{PS}, D_{PI}, and D, where $a_J > a_{J0}$, $D_{PS} > D_{PS,0}$, $D_{PI} < D_{PI,0}$, and $D > D_0$ and also changes in morphology.

The homopolymer HS generally causes the PS domains to swell both laterally and longitudinally, causing an expansion of average distance between chemical junctions from a_{J0} to a_J, a change in domain sizes from D_0 to D, $D_{PS,0}$ to D_{PS}, and $D_{PI,0}$ to D_{PI}, and a change in the domain morphology. The lower the value of $M_{n,homo}$, the more uniform is ϕ_{homo} and the greater is the expression of a_J, which, in turn, causes increasing reduction of D_{PI} and less increase of $D = D_{PI} + D_{PS}$. Upon solubilization of HS, the thickness of the PI lamella decreases from $D_{PI,0}$ to D_{PI} to maintain the bulk density. Further increase of ϕ_H causes further reduction of D_{PI}, which causes a greater degree of compression on the molecular conformation of the PI block chains and hence an increasing penalty on the conformational free energy of the PI block chains. This penalty on the conformational free energy is the driving force for the morphological transition from lamellar to cylindrical microdomains with increasing ϕ_H. The packing of PI block chains inside the curved interfaces in the cylindrical microdomains gives less penalty on the conformational free energy compared with the packing with the flat interfaces in the lamellar microdomains. The cylindrical domains with the curved interface cause a cost of free energy to bend the interface. If this cost of the bending free energy is outweighed by the gain of the conformational free energy, the morphological transition occurs from the lamella to the cylinder, as found in our experiments (Figure 2). The uniform solubilization of HS causes further stretching of PS block chains normal to the interface, and the uniformly solubilized HS also has a conformation stretched and squeezed in the directions, perpendicular and parallel to the interface, respectively.[16] This occurs because the uniformly solubilized HS chains are in the same field as that exerted by the block polymer chains.

Within the range of the large $M_{n,homo}$ covered in this work, the solubilization of HS is localized as exaggerated in the schematic diagram shown in Figure 12d. Here HS causes no lateral swelling of PS domains so that a_J is nearly equal to a_{J0} and the PI domains are not affected by the solubilization, i.e., $D_{PI} \cong D_{PI,0}$, and the lamellar morphology is conserved (see the results for HY-8 and HY-8/517 in Table III). HS causes only the longitudinal swelling of PS domains and an increase of D_{PS} from $D_{PS,0}$. Thus for a given ϕ_H, D in this range is expected to be much larger than that in the range of the uniform solubilization as is experimentally observed in Figure 7. For $\phi_H = 1 - \phi_{block} = 0.5$ the solubilization behavior changes from uniform to localized solubilization, with increasing $M_{n,homo}$, as shown schematically in Figure 12b–d, which would then cause the change of morphology from cylindrical to lamellar microdomains, as observed in Figure 2. It is conceivable that the locally solubilized HS as in Figure 12d has a conformation quite different from that for the uniformly solubilized HS; viz., the conformation is squeezed in the direction normal to the interface, as sketched in Figure 12d.

The change of the solubilization behavior is a consequence of the effect of $M_{n,homo}$ on miscibility between HS homopolymers and PS block chains. Since the PS block chains are *confined chains* with one end fixed at the interfaces and with their segments restricted in the PS domain space, the mixing of these confined PS chains with HS involves a significant *loss of the conformational entropy* in both the free chains (HS) and the confined chains (PS). Obviously the loss of the conformational entropy increases with increasing $M_{n,homo}$. Hence the larger the value of $M_{n,homo}$, the less miscible are HS and PS, and hence HS chains tend to be localized or segregated in the middle of the PS domains or segregated out from the microdomain system to form a macroscopic phase. This system offers a good and clear-cut example that *the confined chains are less miscible with corresponding free chains.*

Acknowledgment. We are grateful to Dr. M. Whitmore and Dr. J. Noolandi for useful discussions and to TOSOH Co., Ltd., for providing homopolystyrene samples used in this work. This work was supported in part by a Grant-in-Aid for Scientific Research (63470090) from the Ministry of Education, Science and Culture, Japan. This work was also supported by a research grant from Mitsubishi Kasei Corp.

References and Notes

(1) Tanaka, H.; Hasegawa, H.; Hashimoto, T. *Macromolecules*, in press.
(2) Quan, X.; Gancarz, I.; Koberstein, J. T.; Wignall, G. D. *Macromolecules* **1987**, *20*, 1434.
(3) Quan, X.; Gancarz, I.; Koberstein, J. T.; Wignall, G. D.; Wilson, F. C. Preprint, "Spatial Distribution of Homopolymer Chains in a Block Copolymer Matrix". In Abstracts of the Materials Research Society, December 1986.
(4) Shibayama, M.; Hashimoto, T.; Hasegawa, H.; Kawai, H. *Macromolecules* **1983**, *16*, 1427. Mori, K.; Hasegawa, H.; Hashimoto, T. *Polymer*, in press.
(5) Hashimoto, T.; Nagatoshi, K.; Todo, A.; Hasegawa, H.; Kawai, H. *Macromolecules* **1974**, *7*, 364.
(6) Shibayama, M.; Hashimoto, T. *Macromolecules* **1986**, *19*, 740.
(7) Hashimoto, T.; Harada, M., paper in preparation.
(8) Hong, K. M.; Noolandi, J. *Macromolecules* **1983**, *16*, 1083.
(9) Whitmore, M. D.; Noolandi, J. *Macromolecules* **1985**, *18*, 2486.
(10) Zin, W.-C.; Roe, R.-J. *Macromolecules* **1984**, *17*, 189.
(11) Mori, K.; Tanaka, H.; Hashimoto, T. *Macromolecules* **1987**, *20*, 381.
(12) Tanaka, H.; Hashimoto, T. *Polym. Commun.* **1988**, *29*, 212.
(13) Hashimoto, T.; Tanaka, H.; Hasegawa, H. In *Molecular Conformation and Dynamics of Macromolecules in Condensed Systems*; Nagasawa, M., Ed.; Elsevier: Amsterdam, 1988.

(14) Hashimoto, T.; Shibayama, M.; Kawai, H. *Macromolecules* **1980**, *13*, 1237.
(15) The paracrystal analyses give $\Delta D = gD = 4.1$ nm, and hence the standard deviation of the thickness of PS lamellae $\sigma_{PS} = (\Delta D^2 - \sigma_{PI}^2)^{1/2} = 4.0 \text{ nm} > \sigma_{PI}$. The relative standard deviations for PS and PI lamellae, however, are about equal; $\sigma_{PS}/D_{PS} = 4.0/51.0 \times 0.735 = 0.1$ and $\sigma_{PI}/D_{PI} = 0.07$.
(16) Hasegawa, H.; Tanaka, H.; Hashimoto, T.; Han, C. C. *J. Appl. Cryst.*, in press.
(17) Note added in proof: This is clear because D_{PI} for the neat SI is nearly identical with that for the 50/50 wt/wt mixture as shown in Table III. The conformation changes of both HS and PS block chains are also expected to be small, even if there were to some extent.